International Journal of Thermophysics, Vol. 27, No. 1, January 2006 (© 2006)
DOI: 10.1007/s10765-006-0040-7

Importance of Third Virial Coefficients for Representing the Gaseous Phase Based on Measuring PVT-Properties of 1,1,1-Trifluoroethane (R143a)[1]

K. Ichikura,[2] Y. Kano,[2] and H. Sato[3, 4]

For a reliable derivation of the thermodynamic properties in the gaseous phase from thermodynamic equations of state, it has been pointed out that third virial coefficients significantly affect calculations of heat capacities. Among existing equations of state including internationally accepted equations, there is a large discrepancy, sometimes more than 5%, in calculated heat-capacity values near saturation. Two different approaches have been conducted in addressing this problem. One is for providing the third virial coefficient from intermolecular-potential models based on speed-of-sound measurements with a spherical resonator, and another is for confirming the effect of the third virial coefficient on density values near saturation by measuring the density precisely with a magnetic suspension densimeter. This report is focused on the latter case, i.e., precise measurements of density for 1,1,1-trifluoroethane, R143a, near saturation and some important evidence for the necessity of considering third virial coefficients for calculating reliable thermodynamic properties in the gaseous phase.

KEY WORDS: density; HFC refrigerant; R143a; saturation; specific heat; third virial coefficient.

[1] Paper presented at the Seventh Asian Thermophysical Properties Conference, August 23–28, 2004, Hefei and Huangshan, Anhui, P. R. China.

[2] Graduate School of Science and Technology, Keio University, 3-14-1 Hiyoshi, Kohoku-ku, Yokohama 223-8522, Japan.

[3] Department of System Design Engineering, Keio University, 3-14-1 Hiyoshi, Kohoku-ku, Yokohama 223-8522, Japan.

[4] To whom correspondence should be addressed. E-mail: hsato@sd.keio.ac.jp

1. INTRODUCTION

It was pointed out by Narukawa et al. [1] from our group in 2000 that a large discrepancy (sometimes more than 5%) exists among calculated values of the specific heat capacity in the gaseous phase near saturation from existing equations of state developed for hydrofluorocarbons. Our group has also pointed out that the behavior of second and third virial coefficients may affect the discrepancy. Especially the third virial coefficients derived from existing equations of state show different behavior at low temperatures. Many efforts have been made experimentally and theoretically to determine the virial coefficients in the past. But no one knows the correct quantitative third virial coefficient or the process to determine it from theoretical or experimental information. Two different methods for determining the third virial coefficient are investigated by our group: a method using intermolecular-potential models with four parameters including a temperature-correction parameter determined on the basis of speed-of-sound measurements by Kojima [2], as well as by others [3–5], and a method to determine it from precise PVT measurements in the vicinity of saturation.

We precisely measured PVT-properties of R143a in the region near saturation for the gaseous phase with a magnetic suspension densimeter developed in the laboratory of Wagner and his co-workers [6]. On the basis of our measurements near saturation, we showed that most of the existing equations of state do not represent the measurements well. There are obviously systematic deviations in the region near saturation from existing equations of state. The reason is that they have been developed without the experimental data measured in the vicinity of saturation. First, a virial equation of state based on our PVT measurements will be introduced. The virial equation of state enables one to represent thermodynamic property values including density, speed of sound, and specific heat capacity in the gaseous phase including the region near saturation. Second, the importance of the third virial coefficient in representing thermodynamic surfaces in the gaseous phase especially near saturation will be demonstrated in this paper.

2. EXPERIMENTAL APPARATUS

Two densimeters with a magnetic suspension balance are used for density measurements. The details of the densimeter were introduced by Klimeck et al. [6]. The apparatus (shown in Fig. 1) was assembled by our group for measuring PVT properties of fluids including those near saturation in both the liquid and gaseous phases. This apparatus consists of a

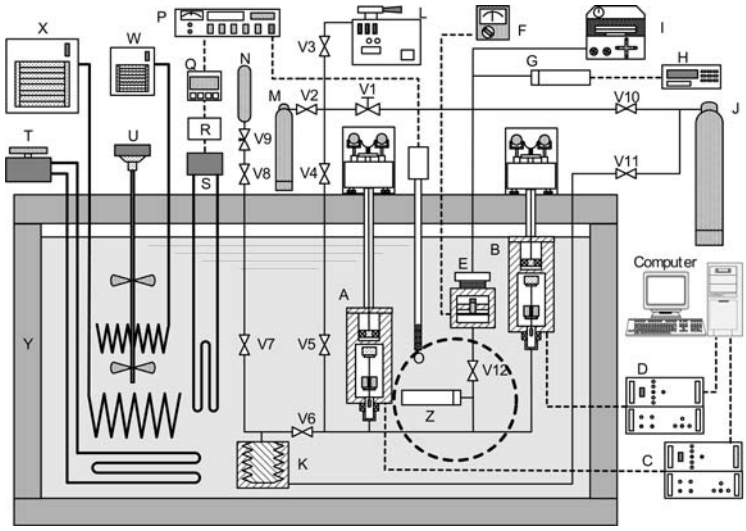

Fig. 1. Experimental apparatus. (A) Densimeter with magnetic suspension balance for liquid, (B) densimeter with magnetic suspension balance for gas, (C) control box for [A], (D) control box for [B], (E) differential pressure detector, (F) circuit tester, (G) quartz pressure transducer, (H) pressure computer, (I) dead weight pressure gauge, (J) nitrogen gas bomb, (K) variable volume vessel with metallic bellows, (L) vacuum pump, (M) argon gas bomb, (N) sample cylinder, (O) standard platinum resistance thermometer, (P) thermometer bridge, (Q) PID controller, (R) thyristor regulator, (S) sub-heater, (T) main heater, (U) stirrer, (V1–V11) valves, (W) sub-cooler, (X) main cooler, (Y) thermostatic bath, and (Z) quartz pressure transducer.

temperature control/measurement system, a pressure control/measurement system, and a density measurement system.

We recently introduced a quartz digital pressure gauge (Z) covered with a container as shown in Fig. 1. The quartz digital pressure gauge was calibrated by using a dead-weight pressure gauge (Model 5201, DH Instruments). Pressure was indirectly measured through a diaphragm-type differential-pressure detector (E). The uncertainty of pressure measurements is improved from 1.20 kPa to 0.82 kPa by introducing the new pressure gauge. The temperature is measured by a standard platinum resistance thermometer. The thermometer was calibrated on the basis of IPTS-68, and the temperature values were processed in accordance with ITS-90. It was installed at the middle level between two cells of the densimeters of A and B in the thermostatic bath. A density-measurement system is a set of two magnetic suspension densimeters.

The combined standard uncertainties of temperature and pressure measurements are estimated to be not greater than 10 mK and 0.82 kPa, respectively. The uncertainty of the density measurement is estimated to be not greater than 0.03% + 0.005 $kg \cdot m^{-3}$ in density. The sample purity of R143a was 99.99 mass% according to calibration by the manufacturer.

3. EXPERIMENTAL RESULTS

In order to confirm the reliability of the apparatus, density measurements for Ar and CO_2 were carried out. We have 48 *PVT*-properties of Ar and 40 *PVT*-properties of CO_2 in the range of temperature from 283 to 313 K and of pressure from 500 kPa to 3 MPa. All of our measurements for Ar along four isotherms agree with the reliable equation of state developed by Tegeler et al. [7] within the uncertainty of the density measurements. The same reliability was confirmed for CO_2.

After confirming the reliability, we measured 102 *PVT*-properties of R143a in the range of temperature from 283 to 313 K and of pressure from 150 kPa to 1.8 MPa. The actual data values will be reported in Ref. 8. Figure 2 shows deviations of the selected *PVT*-properties from the equation of state developed by Lemmon and Jacobsen [9], which is an internationally accepted equation for R143a recommended by the International Energy Agency (IEA). Most of our measurements are well represented, within $\pm 0.1\%$, which is the uncertainty of the equation of state. Our measurements are compared with four different equations of state in Fig. 3. The baseline is each equation of state in Fig. 3. Those equations of state were developed by Lemmon and Jacobsen [9], Li et al. [10], Span [11], and Outcalt and McLinden [12]. As shown in Fig. 3, the deviations of our density measurements show systematic trends when approaching close to saturation at higher pressures. Although the deviations of the data compared to the equation of state developed by Lemmon and Jacobsen [9] are not significant, other equations of state do not represent our measurements near saturation well.

4. VIRIAL EQUATION OF STATE

We measured 102 *PVT*-properties of R143a in the region near saturation along four isotherms. Based on our *PVT* measurements, we fitted parameters for the density-explicit virial equation of state,

$$Z = \frac{P}{\rho R T} = 1 + B(T)\,\rho + C(T)\,\rho^2, \tag{1}$$

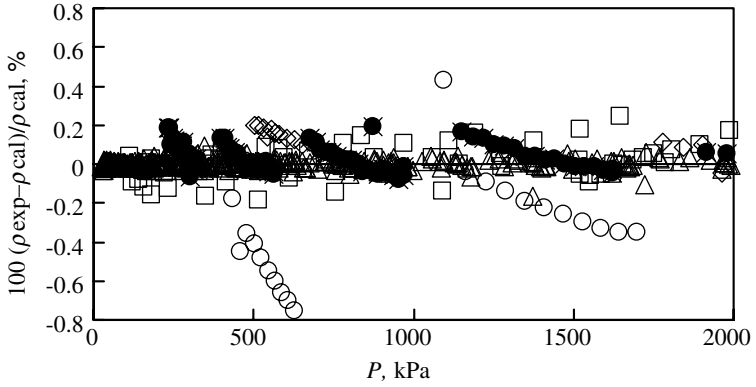

Fig. 2. Relative density deviations of the selected *PVT* measurements from the equation of state developed by Lemmon and Jacobsen [9]. ●, This work; △, de Vries; □, Zhang et al.; ◇, Giuliani et al.; ◯, Fujiwara and Piao; ×, Weber et al.

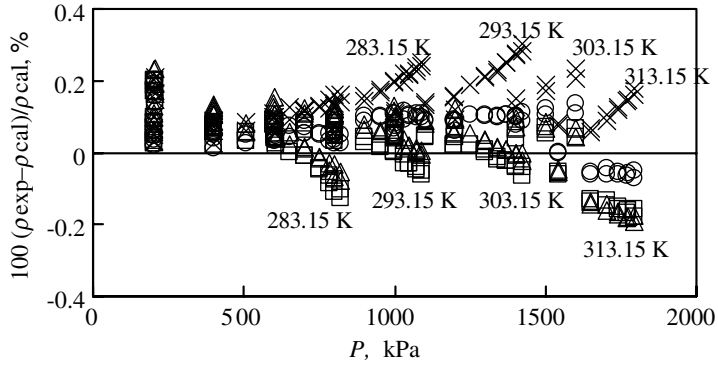

Fig. 3. Relative density deviations of the measurements near saturation in this work from existing equations of state for R143a. ◯, Lemmon and Jacobsen same as shown in Fig. 2; □, Li et al.; △, Span et al.; ×, Outcalt and McLinden.

where Z denotes the compressibility factor; P is the pressure in kPa; T is the temperature in K; ρ is the density in $\mathrm{kg \cdot m^{-3}}$; and $R = 8.314472$ $\mathrm{J \cdot mol^{-1} \cdot K^{-1}}$, the universal gas constant. The second, $B(T)$, and third, $C(T)$, virial coefficients are given by the following functions of temperature:

$$B(T) = b_1 + b_2 T_r^{-1} + b_3 \exp(T_r^{-1}), \tag{2}$$

$$C(T) = c_1 + c_2 T_r^{-\alpha} + c_3 T_r^{-\beta}. \tag{3}$$

In Eqs. (2) and (3), T_r is the reduced temperature defined as T/T_c, whereas b_1 to b_3, c_1 to c_3, α, and β are numerical coefficients. We adopted the critical temperature measured by Aoyama et al. [13]. The numerical coefficients and the critical temperature for Eqs. (2) and (3) are given in Table I. These functional forms have been used in our group since 1995 when Zhang et al. [14] proposed them.

Although the virial equation of state represents the measurements well in the range where our data exist, it becomes less reliable in the region where it is far from our measurements. In order to make it reliable even in the extended range from our measurements, we tried to introduce theoretical second and third virial coefficients deduced from the following cluster integrals of the intermolecular potential energy,

$$B(T) = -\frac{N_A}{2V} \iint f_{12} dr_1 dr_2, \tag{4}$$

$$C(T) = -\frac{N_A^2}{3V} \iiint f_{12} f_{23} f_{31} dr_1 dr_2 dr_3, \tag{5}$$

where N_A is Avogadro's number, V is the molar volume, and f_{ij}, introduced by Mayer and his coworkers [15] due to Hirschfelder et al. [16], is defined as

$$f_{ij} = \exp\left(-\frac{u_{ij}}{\kappa_B T}\right) - 1, \tag{6}$$

u_{ij} is an intermolecular potential energy between molecules i and j, which depends on their separation distance of r_k, and $\kappa_B (= R/N_A)$ is the Boltzmann constant. The details of the intermolecular potential model are also reported by Kojima [2] and by Yasui et al. [5] from our group. Kojima pointed out that it is effective for calculating virial coefficients from an

Table I. Numerical Coefficients and Critical Temperature of Eqs. (2) and (3)

b_1	5.71751×10^{-3}
b_2	-9.26707×10^{-5}
b_3	-3.28792×10^{-3}
c_1	-3.22403×10^{-6}
c_2	9.06716×10^{-6}
c_3	-1.45994×10^{-6}
α	3.0
β	7.0
T_c (K)	345.86

intermolecular potential model with the aid of introducing a temperature-correction parameter of τ as $(T-\tau)$ instead of using temperature T. We also applied τ in developing a new virial equation. For the intermolecular potential model, we selected the Stockmayer potential that has a dipole-dipole interaction term in addition to the Lennard-Jones potential. $B(T)$ and $C(T)$ are theoretically derived from the Stockmayer potential model by the following relations [17]:

$$B(T) = b_0 \left(\frac{4}{T^*}\right)^{1/4} \left[\Gamma\left(\frac{3}{4}\right) - \frac{1}{4}\sum_{n=1}^{\infty}\sum_{l=0}^{n/2} \frac{2^n G_l}{n!}\binom{n}{2l} \times \Gamma\left(\frac{2n-2l-1}{4}\right) t^{*2l} T^{*-(n+l)/2}\right], \tag{7}$$

$$G_l = \frac{1}{8\pi}\int_0^{2\pi}\int_0^{\pi}\int_0^{\pi} \left[g\left(\theta_i, \theta_j, \phi_{ij}\right)\right]^{2l} \sin\theta_i \sin\theta_i d\theta_i d\theta_j d\phi_{ij} = \frac{1}{1+2l}\sum_{m=0}^{l}\binom{l}{m}\frac{3^m}{1+2m}, \tag{8}$$

$$t^* = \frac{\mu_i \mu_j}{2\sqrt{2}\varepsilon_{ij}\sigma_{ij}^3}, \tag{9}$$

$$T^* = \frac{\kappa(T-\tau)}{\varepsilon}, \tag{10}$$

$$b_0 = \frac{2}{3}\pi N_A \sigma^3, \tag{11}$$

$$C(T) = b_0^2\left[\sum_{j=0}^{\infty} c^{(j)} T^{*-(j+1)/2} + \frac{3}{2}\sum_{n=2}^{\infty}\sum_{m=2}^{n}\frac{2^n}{n!}\binom{n}{m}\frac{t^{*m}}{T^{*(n/2+m/4+1/2)}} Q_{mn}^{(j)}\right]. \tag{12}$$

The numerical parameters of Eqs. (7)–(12) were determined on the basis of our measurements and are given in Table II.

Table II. Numerical Parameters of Eqs. (7)–(12)

σ(Å)	5.15049
ε/κ(K)	194.82
t^*	0.47399
τ(K)	53.620

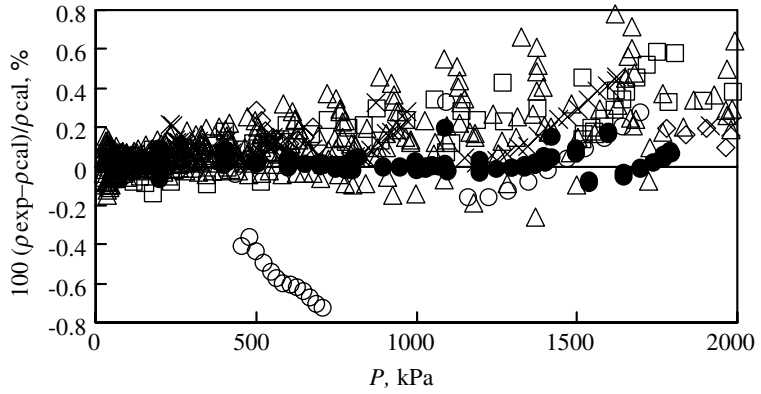

Fig. 4. Relative density deviations of the selected *PVT* measurements from the virial equation, having an empirical background, Eqs. (2) and (3). ●, This work; △, de Vries; □, Zhang et al.; ◇, Giuliani et al.; ◯, Fujiwara and Piao; ×, Weber et al.

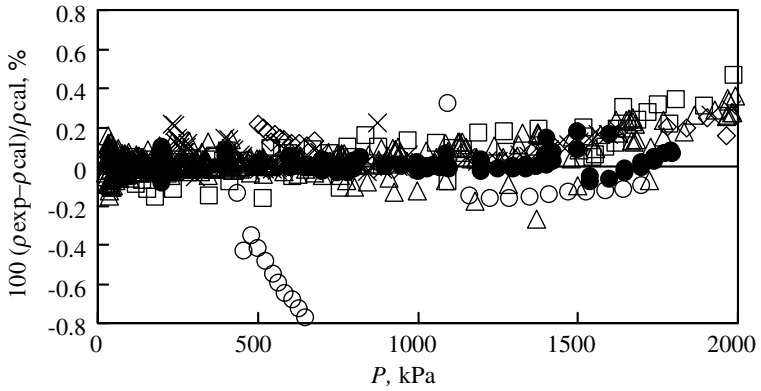

Fig. 5. Relative density deviations of the selected *PVT* measurements from the virial equation having a theoretical background, Eqs. (7)–(12). ●, This work; △, de Vries; □, Zhang et al.; ◇, Giuliani et al.; ◯, Fujiwara and Piao; ×, Weber et al.

Figures 4 and 5 show the deviations of the *PVT* properties from the virial equation of state developed in this study. Both virial equations of state were developed on the basis of a common database, our 102 precise measurements for R143a. It is obvious that the deviations of our measurements from both equations do not exceed ±0.2% and that most of the data are represented within ±0.1%. Both equations of state can represent input data with almost the same reproducibility in the region near saturation. For other measurements [18–22], the theoretical-background (TB)

equation consisting of Eqs. (7)–(12) reproduces the data better than does the empirical-background (EB) equation which consists of Eqs. (2) and (3). The TB-equation represents the measurements by de Vries [18] which are reliable within ±0.2% in the range of pressures below 1.5 MPa and densities below 70 $kg \cdot m^{-3}$, while the deviations from the EB equation exceed 0.4% at higher pressures beyond 1 MPa.

The deviations of accurate speed-of-sound measurements in the gaseous phase from the two virial equations of state are shown in Figs. 6 and

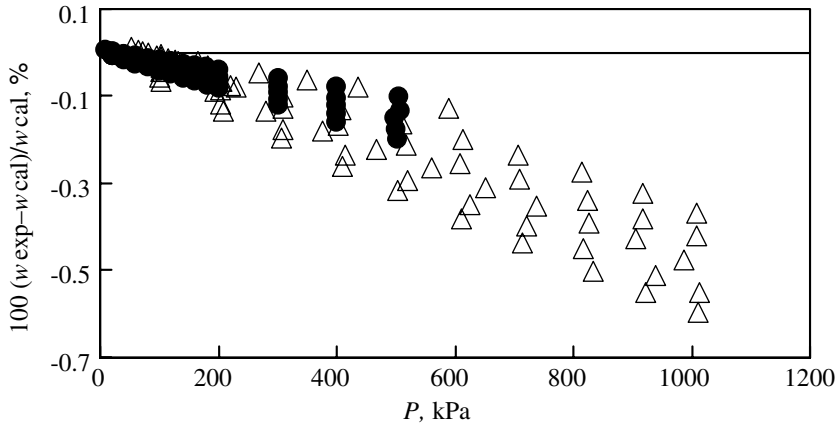

Fig. 6. Relative deviations of the selected speed-of-sound measurements from the empirical-background (EB) virial equation, Eqs. (2) and (3). △, Gillis et al.; ●, Ogawa et al.

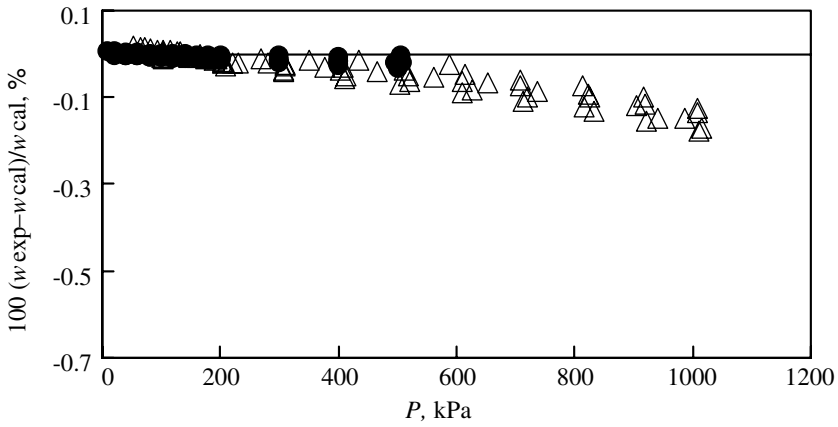

Fig. 7. Relative deviations of the selected speed-of-sound measurements from the theoretical-background (TB) virial equation, Eqs. (7)–(12). △, Gillis et al.; ●, Ogawa et al.

7. The speed-of-sound measurements were reported by Ogawa et al. [23] and Gillis et al. [24]. The TB-equation also represents the measurements better than does the EB-equation as shown in Figs. 6 and 7.

Thermodynamic properties derived from the TB-equation are reliable in the gaseous phase, at least in the region where the measured data are available as introduced above. In addition, the equation should be reliable in the gaseous phase including the region where no measured data are available because it behaves in the same manner as the theoretical behavior determined from the intermolecular potential model. In the following section, reliabilities of the derived specific heats and the virial coefficients will be discussed.

5. IMPORTANCE OF THIRD VIRIAL COEFFICIENT

The isochoric, c_v, and isobaric heat-capacity, c_p, values derived from different equations of state are compared along some isobars in Figs. 8 and 9. Vapor pressures and ideal-gas heat capacities, c_p^0, for calculating c_v and c_p of the saturated vapor are calculated from a vapor–pressure equation developed by Matsuda et al. [25] and from a c_p^0 equation reported by Sato et al. [26]. As shown in Figs. 8 and 9, the isobaric lines calculated

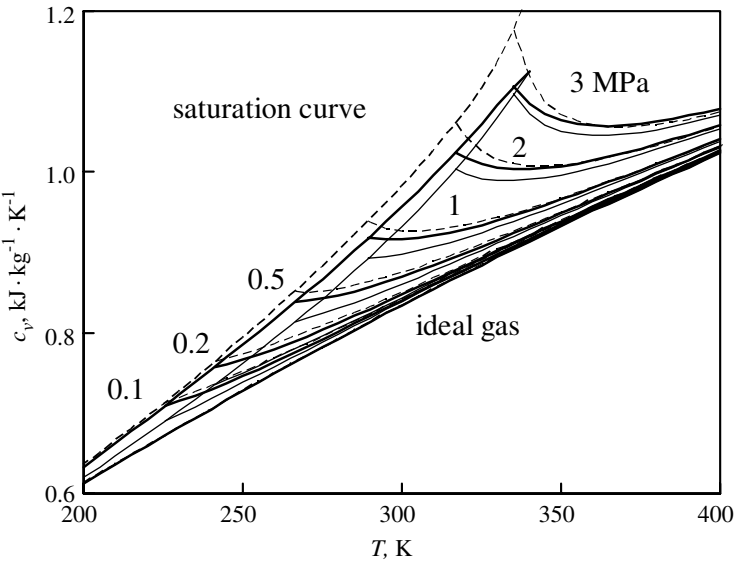

Fig. 8. Isochoric heat capacities, c_v, along different isobars. Thick solid line, the TB-virial equation of state; thin solid line, the EB-virial equation of state; dashed line, equation of state by Lemmon and Jacobsen.

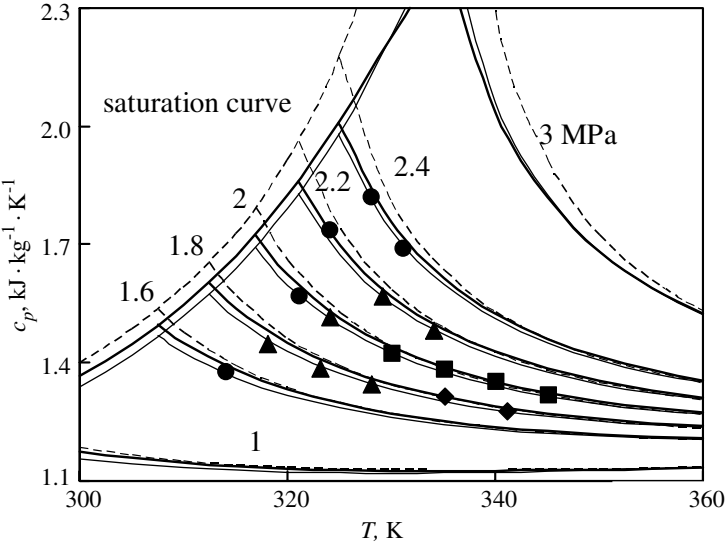

Fig. 9. Isobaric heat capacities, c_p, along different isobars. Thick solid line, the TB-virial equation of state; thin solid line, the EB-virial equation of state; dashed line,equation of state by Lemmon and Jacobsen; ●, Yasumoto; ▲, Takei et al.; ■, Mukoyama; ♦, Nakashima.

from the equation of state by Lemmon and Jacobsen have steeper curvature than those from our virial equations of state. The greatest difference in the behavior of heat capacities appears at saturation. In the case of the isobaric specific heat, the measurements by Mukoyama [27], Nakashima [28], Takei et al. [29], and Yasumoto [30] are available which are compared with the equations of state in Fig. 9. Figure 9 shows that our virial equations of state represent all of the measurements better than does the equation of state by Lemmon and Jacobsen.

As mentioned previously, our group has consistently pointed out that there are large differences among the specific-heat values derived from existing equations of state in the region near saturation and that the behavior of the third virial coefficients may affect the difference. Figures 10 and 11 show the temperature dependence of the second and third virial coefficients, respectively. The data plotted in these figures are theoretically calculated from the Stockmayer potential model by Yokozeki et al. [31]. The behavior is only qualitative since the second and third virial coefficients do not reproduce the physical thermodynamic value with appropriate reliability. Regarding the second virial coefficient, all models including those by Yokozeki et al. agree well with each other except at lower temperatures where only

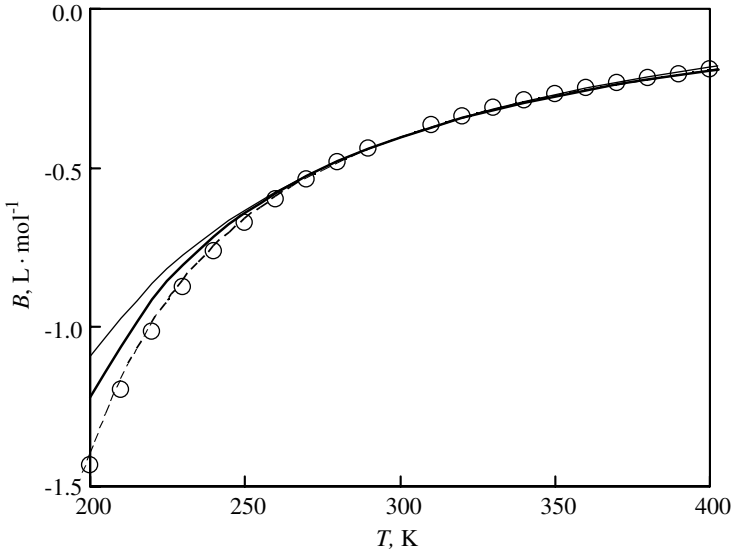

Fig. 10. Temperature dependence of the second virial coefficients of equations of state. Thick solid line, the TB-virial equation of state; thin solid line, the EB-virial equation of state; dashed line, equation of state by Lemmon and Jacobsen; ○, calculation from Stockmayer potential model by Yokozeki et al.

the equation of state by Lemmon and Jacobsen agrees well with the data by Yokozeki et al. Although the difference among second virial coefficients increases at lower temperatures, the specific-heat values derived from these three equations of state are getting closer to each other at lower temperatures as shown in Fig. 8.

Regarding the third virial coefficient, there are also large differences at lower temperatures among the different thermodynamic models. Our third virial coefficients both in TB- and EB-virial equations of state have the maximum around 250 K, while that from the equation of state by Lemmon and Jacobsen continues to rise as the temperature is reduced.

The importance of obtaining accurate third virial coefficients is because they strongly affect the thermodynamic properties in the region near saturation, even at higher temperatures as shown in Figs. 8 and 9 for the specific heats.

For ascertaining the role of the third virial coefficients, a virial equation of state having only the second virial coefficient was developed. Deviations of our PVT measurements from the two different virial equations of state are simultaneously shown in Fig. 12; circles show deviations from the equation having both second and third virial coefficients with the

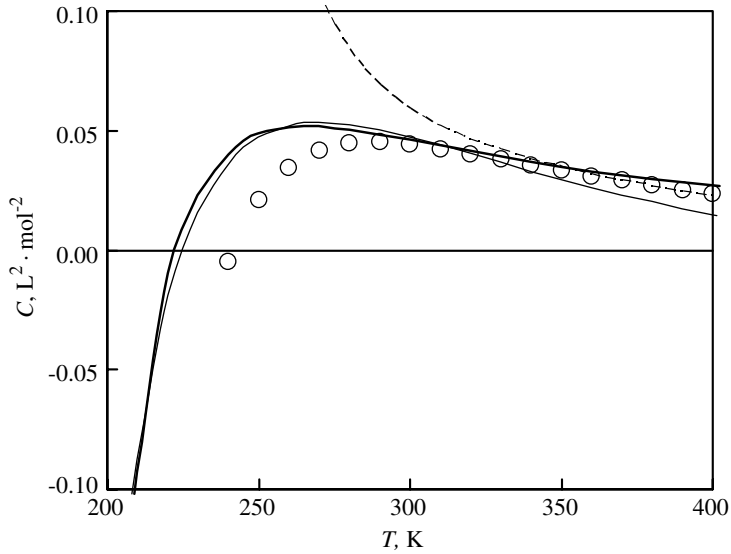

Fig. 11. Temperature dependence of the third virial coefficients of equations of state. Thick solid line, the TB-virial equation of state; thin solid line, the EB-virial equation of state; dashed line, equation of state by Lemmon and Jacobsen; ◯, calculation from Stockmayer potential model by Yokozeki et al.

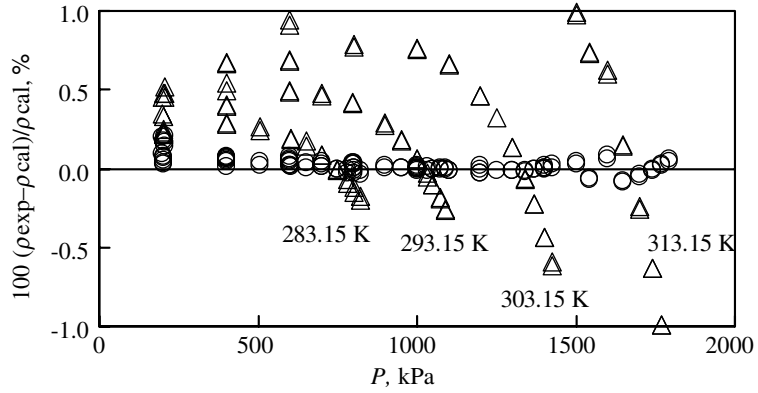

Fig. 12. Relative deviations of our *PVT* measurements from the virial equation developed. ◯, virial equation of Eqs.(7) – (11); △, virial equation having only second virial coefficient in Eq. (1).

numerical parameters of Table II, and triangles show deviations from the virial equation of state having only second virial coefficients with the numerical parameters of Table III. As shown in Fig. 12, the virial equation

Table III. Numerical Parameters of Eqs. (7)–(11) for Case of Equation Having Only Second Virial Coefficients

σ(Å)	7.93008
ε/κ(K)	99.910
t^*	1.1793
τ(K)	−19.925

of state using only the second virial coefficient does not represent our measurements well, and the deviations of our density measurements systematically deviate from the equation. The deviations increase systematically close to saturation at higher pressures.

In addition, comparisons of the isochoric, c_v, and isobaric heat-capacity, c_p, values derived from the two different virial equations of state are shown in Figs. 13 and 14. The c_v and c_p values derived from the two different virial equations of state have the largest discrepancies at saturation. This shows the importance of accurate third virial coefficients in calculating the thermodynamic properties near saturation.

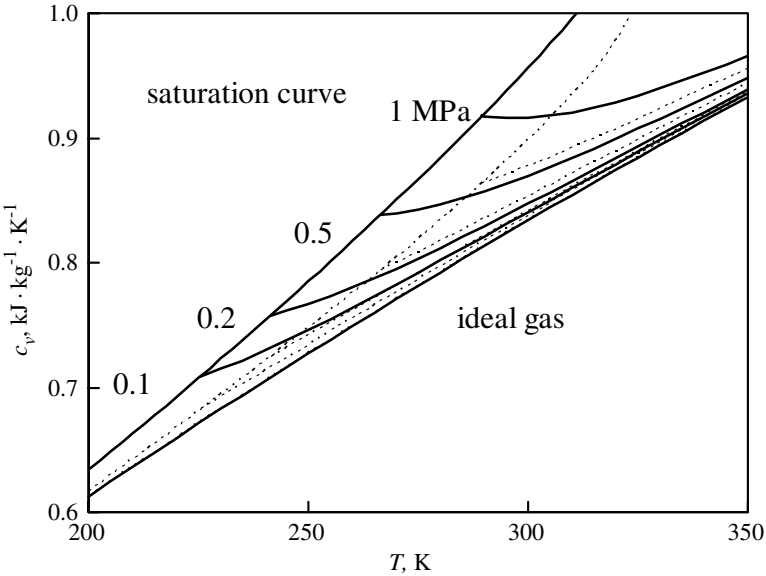

Fig. 13. Isochoric heat capacity, c_v, along different isobars. Thick solid line, virial equation of Eqs.(7)–(12); dashed line, virial equation having only second virial coefficient in Eq. (1).

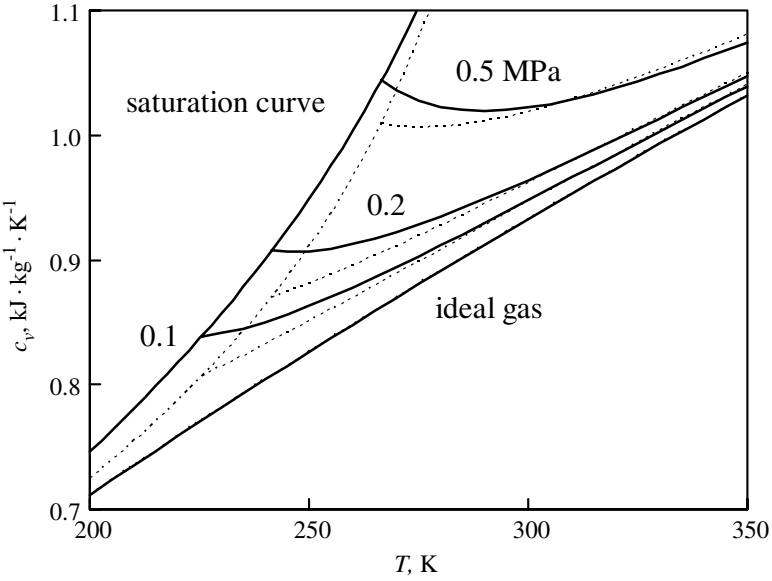

Fig. 14. Isobaric heat capacity, c_p, along different isobars. Thick solid line, virial equation of Eqs.(7)–(12); dashed line, virial equation having only second virial coefficient in Eq. (1).

6. CONCLUSION

We measured precise *PVT* properties of R143a in the gaseous phase including near saturation with a magnetic suspension densimeter. We successfully obtained 102 *PVT*-properties with an uncertainty of $\pm(0.03\% + 0.005\,\mathrm{kg \cdot m^{-3}})$. Based on the precise measurements obtained near saturation, the parameters of the Stockmayer potential model with a new parameter proposed by Kojima were determined. Then, a new virial equation of state using the second and third virial coefficients deduced from the Stockmayer potential model was developed which enabled not only representation of the measurements including density, speed of sound, and specific heat capacity, but also prediction of properties in the range where no experimental data are reported.

By using the Stockmayer potential model and the reliable experimental *PVT*-property data measured in this study, the second and third virial coefficients were determined for R143a. We believe that the virial equation of state developed in this study can provide a reasonable thermodynamic surface for the gaseous phase including near saturation and at lower temperatures. Finally, we would like to strongly point out that the third virial

coefficient has a great influence on the thermodynamic properties near saturation in the gaseous phase.

REFERENCES

1. K. Narukawa, A. Mizuoka, and H. Sato, presented at *the 14th Symposium on Thermophysical Properties*, Boulder, Colorado (2000).
2. T. Kojima, *Master's Thesis* (Keio University, Yokohama, 2001).
3. K. Ogawa, *Master's Thesis* (Keio University, Yokohama, 1999).
4. K. Okabe, *Master's Thesis* (Keio University, Yokohama, 2005).
5. M. Yasui, K. Okabe, and H. Sato, presented at *the 7th Thermophysical Properties Conference*, Hefei, China (2004).
6. J. Klimeck, R. Kleinrahm, and W. Wagner, *J. Chem. Eng. Data* **30**:1571 (1998).
7. Ch. Tegeler, R. Span, and W. Wagner, *J. Phys. Chem. Ref. Data* **28**:779 (1999).
8. K. Ichikura, Y. Kano, and H. Sato, to be submitted to *J. Chem. Eng. Data*.
9. E. W. Lemmon and R. T. Jacobsen, *J. Phys. Chem. Ref. Data* **23**:521 (2000).
10. J. Li, R. Tillner-Roth, H. Sato, and K. Watanabe, *Int. J. Thermophys*. **20**:1639 (1999).
11. R. Span, *Multiparameter Equations of State, An Accurate Source of Thermodynamic Property Data* (Springer-Verlag, Berlin, Heidelberg, 2000).
12. S. L. Outcalt and M. O. McLinden, *Int. J. Thermophys*. **18**:1445 (1997).
13. H. Aoyama, G. Kishizawa, H. Sato, and K. Watanabe, *J. Chem. Eng. Data* **41**:1046 (1996).
14. H.-L. Zhang, H. Sato, and K. Watanabe, *Proc. 19th Int. Cong. of Refrigeration*, The Hague (1995), p. 622.
15. J. E. Mayer, *J. Chem. Phys.* **5**:67 (1937); J. E. Mayer and P. G. Ackermann, *J. Chem. Phys.* **5**:74 (1937); J. E. Mayer and S. F. Harrison, *J. Chem. Phys.* **6**:87: (1938); S. F. Harrison and J. E. Mayer, *J. Chem. Phys.* **6**:101 (1938); J. E. Mayer and M. G. Mayer, *Statistical Mechanics* (John Wiley, New York, 1940).
16. J. O. Hirschfelder and C. F. Curtiss, *Molecular Theory of Gases and Liquids* (John Wiley, New York, 1954).
17. J. S. Rowlinson, *J. Chem. Phys.* **19**:872 (1951).
18. B. de Vries, DKV, No.55, Forch.-Ber, DKV-Verlang, Stuttgart, Germany (1997).
19. H.-L. Zhang, H. Sato, and K. Watanabe, *J. Chem. Eng. Data* **40**:887 (1995).
20. L. A. Weber and D. R. Defibaugh, *J. Chem. Eng. Data* **41**:1477 (1996).
21. G. Giuliani, S. Kumar, P. Zazzini, and F. Polanara, *J. Chem. Eng. Data* **40**:903 (1995).
22. K. Fujiwara and C.-C. Piao, *Proc. 16th Japan Symp. Thermophys. Props.,* Hiroshima, Japan (1995), p. 161.
23. K. Ogawa, T. Kojima, and H. Sato, *J. Chem. Eng. Data* **46**:1082 (2001).
24. K. A. Gillis, *Int. J. Thermophys*. **18**:73 (1997).
25. N. Matsuda, K. Morita, and H. Sato, *Proc. 22nd Japan Symp. Thermophys. Props.,* Sendai, Japan (2001), p. 52.
26. H. Sato, T. Kojima, and K. Ogawa, *Int. J. Thermophys*. **23**:787 (2002).
27. K. Mukoyama, *Master's Thesis* (Keio University, Yokohama, 1996).
28. A. Nakashima, *Master's Thesis* (Keio University, Yokohama, 1997).
29. Y. Takei and K. Watanabe, *Proc. 21st Japan Symp. Thermophys. Props*., Nagoya, Japan (2000), p. 172.
30. K. Yasumoto, *Master's Thesis* (Keio University, Yokohama, 2002).
31. A. Yokozeki, H. Sato, and K. Watanabe, *Int. J. Thermophys.* **19**:89 (1998).